Baumann, S.; Serra Alfaro, JM.; Lobera González, MP.; Escolástico Rozalén, S.; Schulze-Kueppers, F.; Meulenberg, WA. (2011). Ultrahigh oxygen permeation flux through supported Ba0.5Sr0.5Co0.8Fe0.2O3-delta membranes. Journal of Membrane Science. 377(1-2):198-205. doi:10.1016/j.memsci.2011.04.050

Ultrahigh Oxygen Permeation Flux through Supported $Ba_{0.5}Sr_{0.5}Co_{0.8}Fe_{0.2}O_{3-\delta}$ Membranes

Journal of Membrane Science (2011) (accepted 24/04/2011)
doi: 10.1016/j.memsci.2011.04.050

S. Baumann[1], J. M. Serra[2,*], M. P. Lobera[2], S. Escolástico[2], F. Schulze-Küppers[1], W. A. Meulenberg[1]

[1]*Forschungszentrum Jülich GmbH, Institute of Energy and Climate Research IEK-1, Leo-Brandt-Str. 1, D-52425 Jülich, Germany*

[2]*Instituto de Tecnología Química (Universidad Politécnica de Valencia – Consejo Superior de Investigaciones Científicas), Av. Naranjos s/n, E-46022 Valencia, Spain.*

ABSTRACT

Oxygen transport membranes made of $Ba_{0.5}Sr_{0.5}Co_{0.8}Fe_{0.2}O_{3-\delta}$ (BSCF) were manufactured by tape casting and co-firing. The disk-shaped membranes consisted of a top gastight layer (70 μm thick) and a porous substrate (830 μm thick) with 34% open porosity. The variation of the permeation operation conditions allowed (i) the identification of the different limitations steps in the permeation process, i.e. bulk oxygen ion diffusion, catalytic surface exchange and gas phase diffusion in the membrane compartments and porous substrate; and (ii) the ultimate optimization of the oxygen flux. The variables considered in the systematic permeation study included the inlet gas flow rate of the sweep and air feed, the temperature and the nature of the oxygen feed gas (air or pure oxygen). Moreover, the influence of the deposition of a catalytic activation layer (17 μm thick) made of BSCF on top of the thin gastight layer was investigated. As a result of this parametric study, unpreceded oxygen flux values were achieved, i.e. a maximum flux of 67.7 ml(STP) $min^{-1}cm^{-2}$ was obtained at 1000 ºC using pure oxygen as the feed and argon as the sweep, while a flux of 12.2 ml(STP) $min^{-1}cm^{-2}$ at 1000 ºC was obtained when air was used as the feed.

Keywords: oxygen transport membrane; supported membrane; oxygen flux; BSCF; oxygen separation

* Corresponding author

Fax: +34 963 877809; Tel: +34 963 879448; E-mail: jmserra@itq.upv.es

1. Introduction

One important strategy for reducing CO_2 emissions, while the energy demand is increasing, is carbon capture and storage (CCS). Different fossil fuel power plant concepts for CCS are currently being developed. Examples include post-combustion, pre-combustion and oxyfuel. In oxyfuel power plants, the fossil fuel is combusted using pure oxygen or a nitrogen-free gas stream enriched with oxygen. The result of this concept is an off-gas containing primary CO_2 and H_2O, i.e. 90-95% CO_2 in the dried flue gas. The CO_2 can then be captured more easily than when air is used in the combustion process, which leads to 10-14% CO_2 in the dried flue gas. [1] The oxygen required for this concept can be provided by different methods, of which ceramic oxygen transport membranes* (OTMs) have the lowest efficiency losses [2], especially when recirculated flue gas is used as sweep gas.

OTMs consist of gastight mixed ionic-electronic conductors (MIEC) and allow oxygen diffusion via oxygen vacancies in the crystal lattice. Therefore, the selectivity of the membranes is infinite, which means that they provide pure oxygen. The most promising materials for OTMs are perovskites with the formula $ABO_{3-\delta}$ [3]. In last decade, intensive research has been dedicated to the preparation and characterization of MIEC membranes [4-12]. The materials showing the highest oxygen permeability are based on $Ba_{0,5}Sr_{0,5}Co_{0,8}Fe_{0,2}O_{3-\delta}$ (BSCF), which was first reported by Shao et al. [13] and has attracted great interest recently [14-18]. The thermodynamic driving force for oxygen transport through a MIEC membrane is the oxygen chemical potential gradient along the thickness of the membrane, which is given by the operating conditions. The oxygen permeation flux based on bulk diffusion can be described by the Wagner Equation [3]

$$J_{O_2} = \frac{RT}{16F^2L}\int_{P''_{O2}}^{P'_{O2}} \sigma_{amb}(pO_2)\, d\ln pO_2 \qquad (1)$$

where J_{O2} is the oxygen permeation flux in $mol \cdot m^{-2} \cdot s^{-1}$, R is the gas constant, F is the Faraday constant, L is the membrane thickness, σ_{amb} is the ambipolar conductivity, and pO_2' and pO_2" are the oxygen partial pressures at the high pressure side and low pressure side, respectively.

In order to increase the oxygen permeation flux through a membrane, the thickness should be as low as possible. When the thickness becomes very low, a porous support is needed for mechanical stability, particularly in the case of planar membranes. This has led to recent increased interest in the development of supported membranes. The membranes that have been investigated vary widely in terms of membrane thickness (10 µm to 500 µm) and material [19-26] (table 1). The permeation enhancements that have been reported are normally much less than the values predicted by the Wagner equation (1), assuming direct reciprocal behaviour of membrane thickness and permeation rate. This is due to the fact that Wagner's

* Also called ionic transport membranes (ITMs)

theory is only valid for solid state diffusion; it does not include surface exchange kinetics (O_2 adsorption, dissociation and reduction) or other gas-phase phenomena, which at least partly dominate permeation through thin membranes. Furthermore, a limiting influence of the porous support has to be considered [26].

This work presents the preparation of asymmetric membranes made of BSCF. The systematic study of the membrane operation variables (inlet gas flow rate at the two membrane compartments, temperature and the nature of the oxygen feed gas) and their influence on the oxygen flux is discussed. Moreover, the influence of the application of an activation layer on top of the thin gastight layer is investigated. The oxygen flux is optimized by eliminating the different process limitations step by step.

2. Experimental

2.1. Membrane preparation

Both the membrane layer and the support were manufactured by tape casting using BSCF. This approach has several advantages, such as perfect chemical compatibility and the same thermal expansion of the two layers [22]. The commercial BSCF powder used (Treibacher Industrie AG, Austria) exhibited an average grain size of 1.7 µm. In the support, corn starch (Cargill, Germany) was used as the pore former with a particle size in the range of 2-30 µm [27].

The slurry preparation procedure is shown in figure 1 and was performed according to [28]. Two slurries were prepared: the slurry for the support layer contained 20% corn starch in relation to the total solid content, whereas the slurry for the membrane layer did not contain any pore former. Sequential tape casting was used to prepare the membrane. First, the membrane layer was cast in two steps with a drying step in between using casting gaps of 50 µm and 100 µm, respectively. After drying, the support layer was cast on top of this layer with a casting gap of 1.9 mm. This layer was then dried and the samples were cut out of the green tape, debindered and sintered in air at 1100°C for 3 h.

The oxygen activation layers were prepared via screen printing. The screen printing ink consisted of BSCF powder provided by Fraunhofer IKTS (Hermsdorf, Germany). It was ball-milled in an acetone suspension prior to preparation of the screen-printing inks and an average particle size of 250 nm was achieved. A typical additive containing 94 wt.% terpineol and 6 wt.% ethylene cellulose was used. Further homogenization was conducted using a three-roll mill. In order to complete homogenization, this step was repeated three times. Moreover, graphite (Aldrich) was used as the pore former in the screen-printing ink. The printed layer was sintered at 1010 ºC.

The microstructure was investigated using scanning electron microscopy (SEM) (Zeiss Ultra 55), and elemental analysis was carried out with energy-dispersive X-ray spectroscopy (EDS) (INCA, Oxford). The porosity of the membranes obtained was investigated by light microscopy and quantitative image analysis using commercial software, i.e. ImageJ and analySIS. Gas tightness was measured using He leakage (Pfeiffer vacuum).

2.2. Oxygen flux measurements

Oxygen permeation studies were carried out in a lab-scale quartz reactor. Synthetic air (21% v/v O_2 in the feed stream) or pure oxygen was fed into the oxygen-rich chamber, while argon was used as the sweep gas on the permeate side. Both gases were fed at atmospheric pressure. Inlet gases were preheated in order to ensure the correct gas temperature for contact with the membrane surface. This is particularly important when high gas flow rates are employed. All streams were individually mass flow controlled. The temperature was measured by a thermocouple attached to the membrane. A PID controller maintained temperature variations within 2 ºC of the set point. The samples consisted of gastight supported BSCF membranes and membrane gas leak-free conditions were achieved using gold rings on both sides of the membrane, which were heated to 1010 °C for 4 hours immediately prior to the measurement. The permeate was analysed at steady state by online gas chromatography using a micro-GC Varian CP-4900 equipped with Molsieve5A, Pora-Plot-Q glass capillary, and CP-Sil modules. Membrane gas leak-free conditions were ensured by continuously monitoring the nitrogen concentration in the product gas stream (just before and after switching to a pure O_2 feed). An acceptable sealing was achieved when the ratio between the oxygen flow leak and the oxygen flux was lower than 1%. The data reported here were achieved at steady state after one hour in the reaction stream. Each test was repeated three times to minimize the analysis error. The experimental analytical error was below 0.5 %.

Oxygen permeation was determined in the temperature range of 700-1000 ºC. The results obtained at different operating conditions are shown below. J_{O2} was studied for various sweep gas flow rates (i.e. different oxygen partial pressure on the permeate side, pO_2") and different pO_2' (synthetic air or pure oxygen). Oxygen permeation measurements were carried out with the membrane layer and the support on the sweep and the feed side, respectively. This situation was chosen because concentration polarization limitations in the support can easily be overcome by using pure oxygen as feed. In contrast, it would be impossible to easily eliminate such effects at the sweep side. Therefore, the potential of the thin supported membrane layer and the surface activation layer can be assessed following this approach.

3. Results and Discussion

3.1. Membrane assembly microstructure

A preliminary sintering study of both tapes with different types and amounts of pore formers (support) and tapes without pore former (membrane) was performed aiming at a porous support and a gastight membrane layer, respectively, at the same sintering temperature. The sintering shrinkage of the two tapes has been adapted in such a way that a maximum match existed, leading to low bending of the co-sintered sample tracked by laser topography. The best results were obtained when using 20 wt% corn starch as a pore former and subsequently co-firing at 1100°C for 3 hours in air. For the disk-shaped samples (20 mm in diameter), gas tightness was confirmed by measuring the He leak, revealing a value of $6 \cdot 10^{-6}$ mbar l cm^{-2} s^{-1}.

Figure 2 presents the SEM analysis of fracture cross-sections of the samples after permeation tests. Figure 2a shows an overview of the co-sintered membrane assembly. The porosities of the membrane layer and the support layer were 3% and 34%, respectively, as determined by image analysis. The pore size of the substrates ranged from 5 to 25 μm while the closed pores of the dense membrane layer had an average pore size of approx. 3 μm (see Figure 2b). The BSCF grain size after sintering at 1100ºC was large, typically above 10 μm. A detailed analysis at high magnifications suggested that most of the pores in the top dense layer were occluded in the grain interior and not preferentially located at grain boundaries. The thickness of the gastight membrane layer was 70 μm and it was very homogenous. The whole membrane assembly was 900 μm thick. The substrate was composed of very well-bound and sintered BSCF grains.

The formation of a fine-grain porous layer with a thickness below 100 nm was observed on top of the dense BSCF layer. It was noted that this porous layer was not well attached to the dense membrane surface. This porous layer was not present before the testing and originated during operation, which involved continuous sweeping with argon (although the average oxygen partial pressure was typically above 0.001 due to the high oxygen flux). These surface deposits are most likely caused by fouling, i.e. the deposition of particles (SiO_2, CrO_x, FeO_x, etc.) from the piping, the quartz reactor or the sealing material. The surface segregation of secondary phases from the BSCF bulk [29] may also have taken place. In general, the membranes do not show any apparent degradation or damage.

Figures 2c and 2d show the membrane with an activation layer composed of porous BSCF. The oxygen activation layer had an open microstructure and a homogeneous thickness of 17 μm. Figure 2d and Figure 3 show higher magnification images of the porous layer. The particle size was well below 1 μm and the presence of big planar voids (macropores) was observed. These pores were produced by the incorporation of graphite platelets in the printing

ink and the subsequent removal during sintering. The introduction of such macropores aimed to enhance gas exchange through the layer. Furthermore, the porous layer was found to be stable during the whole high-temperature oxygen permeation measurement.

3.2. Oxygen permeation

3.2.1. Transport mechanisms model

Oxygen permeation comprises a very complex set of different transport mechanisms, which can be interpreted as a series of resistances (Figure 4). Depending on the operating conditions, the driving force can be decreased due to a depletion or accumulation of O_2 in porous layers, i.e. support and activation layers, or even in the gas phases. This gives rise to a lower oxygen concentration gradient in the boundary layer. This phenomenon is referred to as concentration polarization and it has serious detrimental effects in the membrane separation process. In the feed gas, concentration polarization can occur especially at high permeation rates due to oxygen depletion in the gas phase above the support (R_{CP1}). This effect is expected to be even stronger within the pores of the support, where molecular diffusion is the predominant transport mechanism ($R_{SUPPORT}$). At the membrane surface, the oxygen has to adsorb, reduce, and dissociate in order to form oxide ions, which have to incorporate into the perovskite lattice. This multistep process is summarized in one resistance R_{S1}. The oxygen ions diffuse through the perovskite bulk and grain boundary (R_{SOLID}). Then, the multistep surface exchange (R_{S2}) occurs and the oxygen is desorbed. Generally, the gas-phase resistance at the permeate side may be negligible compared to that of solid state diffusion and exchange reactions, but when the oxygen permeation flux is sufficiently high, concentration polarization in the gas phase (R_{CP2}) becomes significant. All of these resistances are dependent on the respective local oxygen partial pressure, which are not directly detectable.

The temperature dependence of the oxygen permeation flux through a bare, supported BSCF membrane was studied (Figure 5) using two different oxygen concentrations in the feed stream, i.e. synthetic air and pure oxygen. The results indicated Arrhenius behaviour although the apparent activation energies ($E_{a,a}$) for oxygen transport changed as a function of feed gas nature and/or temperature, which suggests that the rate-limiting step changes according to the temperature range investigated. This behaviour is characteristic of perovskite-type oxides, such as BSCF. In the high-temperature range, oxygen permeation is typically limited by oxygen ions diffusing through the perovskite bulk and grain boundary, while at lower temperatures it is more limited by surface steps. Moreover the $E_{a,a}$ for oxygen surface exchange is higher than that for the oxygen ion diffusion [3,9,13-15,18]. However, this simplified picture does not properly describe the permeation process in supported membranes (e.g. permeation results in Figure 5) when high oxygen fluxes are obtained. In the present case, all of the mentioned resistances may contribute to the overall process resistance.

3.2.2. Influence of catalytic layer

The membrane surface was modified by depositing a porous activation layer of BSCF aiming to improve the oxygen flux permeated (J_{O2}). The plots in Figure 6 show the oxygen permeation fluxes through the bare membrane and the coated membrane in the temperature range of 700-1000 ºC for different sweep gas flow rates when synthetic air was used as the feed gas. As expected, the results indicated Arrhenius behaviour as a function of the temperature. Specifically, they showed two ranges of apparent activation energy ($E_{a,a}$) for oxygen permeation (an estimation of the $E_{a,a}$ is shown in table 2). The critical temperature for the rate-limiting step change was around 800 ºC. This change was caused by the temperature dependence of the characteristic thickness L_c below which the surface exchange kinetics become more and more rate limiting [3]. The surface exchange kinetics possessed a higher activation energy than solid state diffusion, resulting in a higher apparent activation energy in the low-temperature region. Furthermore, the surface exchange coefficient k increased with increasing p_{O2} [3]. Therefore, catalytic activation was expected to be more effective at the permeate side. At the feed side, part of the porous support acted as an activation layer. The thickness of this active part close to the membrane layer was uncertain. The surface activation performance of the support structure attached to the dense membrane layer depends on whether the oxygen can permeate through the solid (perovskite) and the gas phase of the support. Thus, it changes inherently with the measuring conditions, e.g. T, p_{O2}. In all cases, the presence of a catalytic layer on the membrane permeate side improved the J_{O2} reached and reduced the $E_{a,a}$, especially in the low-temperature range. Several studies have shown that surface modification leads to an improved surface exchange rate and a corresponding increase in the J_{O2}. da Costa et al. increased the J_{O2} obtained with a BSCF hollow fibre after surface modification using noble metals [11, 30]. The application of a porous layer made of a compatible material can also be considered as a way of increasing the area available for the surface exchange reactions [31-35].

3.2.3. Influence of gas flow rates

Oxygen permeation flux is strongly influenced by the increase in gas flow rate. This is attributed to (i) the reduction in the concentration polarization resistance at both membrane sides; and (ii) the increase in the driving force, due to either the higher dilution of the permeated oxygen or the higher pO_2 in the depleted air stream.

When the gas space velocity is increased, the fluidodynamic behaviour of the experimental set-up improves, and the effect of the gas polarization diminishes. Figure 7 shows the oxygen permeation flux reached at 900 ºC at various sweep gas flow rates (Q_{Sweep}) for two air flow rates (Q_{Feed}). In all cases, a rise in the air flow rate led to a significant increase in the J_{O2}. This can be ascribed to a lower gas concentration polarization effect at the air side (R_{CP1}), and better molecular diffusion in the pores of the support (lower $R_{SUPPORT}$) for an increased air flow rate. Moreover, Q_{Sweep} variations influenced the oxygen partial pressure at the permeate side (P''_{O_2}). An increase in Q_{Sweep} reduced P''_{O_2} (i.e. the overall driving force in the permeation process has increased) and improved the fluid dynamics. As a result, the oxygen permeation flux improved substantially with increasing sweep gas flow rates. Moreover,

when R_{CP2} was substantially reduced by increasing Q_{Sweep}, one of the major remaining resistances was R_{S2}, which became limiting. Consequently, the effect of the deposition of a catalytic layer becomes more important with increasing sweep gas flow rates, as can be seen in Figure 6. In addition, Figure 8 (top) shows the oxygen flux obtained with the surface-activated membrane as a function of Q_{Sweep} and temperature. It can be ascertained that the increase in the sweep flow rate is very beneficial for the oxygen permeation, especially at the highest temperatures when the highest oxygen fluxes are reached.

3.2.4. Influence of porous support

Since molecular diffusion is the main transport mechanism in the support pores, the structure of the porous support is crucial for the oxygen permeability in the supported thin-film membranes. Therefore, it is important to evaluate the influence of the support on the oxygen permeation process. Support effects due to the gas transport in the pore system can be excluded when pure oxygen is used instead of air as the feed gas (Figure 8 (bottom) and Figure 9). A tremendous increase in permeation flux was observed when the feed gas was switched from air to oxygen, although the overall oxygen partial pressure gradient ln (pO_2'/pO_2") decreased slightly from 2.05 for air to 1.99 for pure oxygen. The use of pure oxygen as the feed gas allowed preventing limitations ascribed to gas transport through the support (principally $R_{SUPPORT}$) and therefore the results of Figure 9 only reflect the influence of the sweep gas flow rate. Figure 8 shows the stronger effect caused by varying the Q_{Sweep} at high temperatures when pure oxygen is fed into the system (note the log scale), i.e. the increase in J_{O2} is much larger with increasing Q_{Sweep}. In this case, the gas concentration polarization effects on the permeate side (R_{CP2}) may be very severe due to the very high oxygen flux achieved under these conditions. However, at lower temperatures, the improvement was not as good, and it appeared that surface exchange (R_{S2}) limits the process under these conditions.

3.2.5. Optimization of oxygen flux

Taking into account the different transport mechanisms in oxygen permeation through supported BSCF membranes, the best operating conditions were selected. The oxygen permeation measurements were carried out using air or pure oxygen as the feed gas. The latter provides an oxygen partial pressure of 1 atm and, thus, the opportunity to exclude the resistances R_{CP1} and $R_{SUPPORT}$. Furthermore, R_{S1} is minimized since the surface exchange rate ($k \propto p_{O2}^{\,n}$) is maximized. On top of the dense membrane layer, a thin porous oxygen activation layer was applied. This layer consisted of the membrane material BSCF and enabled a decrease in the surface exchange resistance (R_{S2}). Moreover, R_{CP2} was negligible due to the use of high flow rates of the sweep gas. Consequently, the permeation rate increased significantly when the feed gas was changed from air to oxygen. The greater enhancement in the case of oxygen is consistent with the model based on consecutive resistances described above. As the resistances R_{CP1} and $R_{SUPPORT}$ were negligible and R_{S1}

was minimized, surface exchange (R_{S2}) and bulk transport (R_{SOLID}) became more important. The gas concentration polarization (R_{CP2}) limitation at the permeate side would become important when high fluxes are reached. When the highest driving force and gas space velocity were applied, i.e. pure oxygen and 400 ml(STP) min^{-1} of Ar as sweep gas, maximum oxygen permeation rates of 67.7 ml(STP) cm^{-2} min^{-1} and 31.8 ml(STP) cm^{-2} min^{-1} were obtained at 1000 °C for the activated and the non-activated membrane, respectively (Figure 10). These oxygen fluxes are the highest reported to date. The previous best results reported using BSCF [11] and BCFZ [8] were obtained at modest oxygen partial pressures, i.e. air at ambient pressure. The oxygen fluxes obtained proved that it is possible to achieve extremely high electronic and oxide ion currents through the crystalline oxide when the other "external limitations" are removed or at least partially mitigated. Specifically, the equivalent ionic current (J_{O2}/nF) here corresponded to 19.4 A cm^{-2} passing through the thin BSCF film.

These results demonstrate the possibility of industrial application of the supported thin-film perovskite membranes for the separation of oxygen from air, which is needed in the oxyfuel and pre-combustion processes for the removal and capture of CO_2. However, long-term (thermal, chemical, and mechanical) stability under service conditions must be investigated in more detail, especially when the membranes are operated at very high ionic currents.

A further enhancement of the permeation flux is expected when rate limiting effects can be overcome stepwise. It has been shown that both the support and the surface exchange kinetics contribute considerably to the overall rate limitation. Hence, it would be advantageous to increase the support porosity and/or tortuosity as well as improve surface activation. Furthermore, it is expected that reducing the membrane layer thickness, e.g. to 5-10 µm, will further increase the permeation rate, especially when both support and surface activation are optimized. Furthermore, there is an engineering challenge in designing membrane module concepts with minimized resistances due to concentration polarization in the gas phases as well as in the support. In relation to their potential application in oxyfuel processes, new highly permeable and stable materials must be developed to achieve high fluxes using recirculated flue gas as the sweep.

4. Conclusions

The manufacturing method of asymmetric membranes made of BSCF by tape casting was presented. The microstructure of the porous substrate, the gastight top layer and the porous activation layer were characterized by EDS/SEM, while the surface quality and evenness of the membranes was assessed by laser topography. The membrane permeation was thoroughly studied while different operation parameters were varied, i.e. inlet gas flow rate of the sweep and air feed, temperature and nature of the oxygen feed gas. Moreover, the influence of the deposition of a catalytic activation layer on top of the thin gastight layer was investigated. The main findings of this study are as follows:

- The presence of the porous support negatively affects the oxygen flux that permeates through the membrane because it produces a concentration polarization on the air side. Support porosity is a crucial issue in the development of thin membranes with very high oxygen fluxes. The pore system of the ceramic substrate has to be engineered in order to enable fast gas diffusion and prevent limitations due to nitrogen accumulation in the pores.

- High sweep flow rates are needed to alleviate gas concentration limitation due to the oxygen concentration at the permeate side and oxygen depletion at the air feed side.

- The application of porous surface activation layers substantially increases the surface exchange rate and notably improves the permeation rate.

In summary, the oxygen permeation flux can be adjusted by controlling the temperature, oxygen partial pressure gradient, and gas flow rates. J_{O2} of the coated supported BSCF thin film (70 μm membrane disk) reached 67.7 ml(STP) $min^{-1}cm^{-2}$ under O_2/argon (pO_2' = 1) at 1000 ºC, and 12.2 ml(STP) $min^{-1}cm^{-2}$ under air/argon (pO_2' = 0.21) at 1000 ºC. These results constitute a proof of concept of the great potential of thin-film supported OTMs.

Acknowledgement

Financial support from the Spanish Ministry for Science and Innovation (Project ENE2008-06302 and FPI Grant JAE-Pre 08-0058), EU through FP7 NASA-OTM Project (NMP3-SL-2009-228701), and the Helmholtz Association of German Research Centres through the Helmholtz Alliance MEM-BRAIN (Initiative and Networking Fund) is kindly acknowledged. Mrs H. Burlet has contributed to this work with the careful revision of the English language.

References

[1] H. Stadler, F. Beggel, M. Habermehl, B. Persigehl, R. Kneer, M. Modigell, P. Jeschke. Oxyfuel coal combustion by efficient integration of oxygen transport membranes. Int. J. Greenhouse Gas Control 5 (2011) 7-14

[2] M. Czyperek, P. Zapp, H.J.M. Bouwmeester, M. Modigell, K. Ebert, I. Voigt, W.A. Meulenberg, L. Singheiser, D. Stöver, Gas separation membranes for zero-emission fossil power plants: MEM-BRAIN. J. Membrane Sci. 359 (2010) 149–159.

[3] J. Sunarso, S. Baumann, J.M. Serra, W.A. Meulenberg, S. Liu, Y.S. Lin, J.C. Diniz da Costa. Mixed Ionic-Electronic Conducting (MIEC) ceramic-based membranes for oxygen separation. J. Membrane Sci. 320 (2008) 13-41.

[4] H.J.M. Bouwmeester, H. Kruidhof, A.J. Burggraaf, P.J. Gellings. Oxygen semipermeability of erbia-stabilized bismuth oxide. Solid State Ionics, 53-56 (1992) 460-468.

[5] S.J. Skinner, J.A. Kilner. Oxygen diffusion and surface exchange in $La_{2-x}Sr_xNiO_{4+\delta}$. Solid State Ionics 135 (2000) 709-712.

[6] Y. Ji, J.A. Kilner, M.F. Carolan. Electrical properties and oxygen diffusion in yttria-stabilised zirconia (YSZ)-$La_{0.8}Sr_{0.2}MnO_{3\pm\delta}$ (LSM) composites. Solid State Ionics 176 (2005)937-943.

[7] V.V. Kharton, A.V. Kovalevsky, A.P. Viskup, A.L. Shaula, F.M. Figueiredo, E.N. Naumovich, F.M. B. Marques. Oxygen transport in $Ce_{0.8}Gd_{0.2}O_{2-\delta}$ based composite membranes. Solid State Ionics 160 (2003) 247-258.

[8] T. Schiestel, M. Kilgus, S. Peter, K.J. Caspary, H. Wang, J. Caro. Hollow fibre perovskite membranes for oxygen separation. J. Membrane Sci. 258 (2005)1-4.

[9] H. Wang, S. Werth, T. Schiestel, J. Caro. Perovskite hollow-fibre membranes for the production of oxygen-enriched air. Angew. Chem. Int. Ed. 44 (2005) 6909-6909.

[10] C. Buysse, A. Kovalevsky, F. Snijkers, A. Buekenhoudt, S. Mullens, J. Luyten, J. Kretzschmar and S. Lenaerts. Fabrication and oxygen permeability of gastight, macrovoid-free $Ba_{0.5}Sr_{0.5}Co_{0.8}Fe_{0.2}O_{3-\delta}$ capillaries for high temperature gas separation. J. Membrane Sci. 359 (2010) 86-92.

[11] A. Leo, S. Smart, S. Liu, J.C. Diniz da Costa. High performance perovskite hollow fibres for oxygen separation. J. Membrane Sci. doi.:10.1016/j.memsci.2010.11.002.

[12] J.M. Serra, V.B. Vert, O.Büchler, W.A. Meulenberg, H.P. Buchkremer. IT-SOFC supported on mixed oxygen ionic-electronic conducting composites. Chem. Mat. 20 (2008) 3867-3875.

[13] Z. Shao, W. Yang, Y. Cong, H. Dong, J. Tong, G. Xiong, Investigation of the permeation behaviour and stability of a $Ba_{0.5}Sr_{0.5}Co_{0.8}Fe_{0.2}O_{3-\delta}$ oxygen membrane, J. Membrane Sci. 172 (2000) 177-188.

[14] J.F. Vente, S. McIntosh, W.G. Haije, H.J.M. Bouwmeester, Properties and performance of $Ba_xSr_{1-x}Co_{0.8}Fe_{0.2}O_{3-\delta}$ materials for oxygen transport membranes, J. Solid State Electrochemistry 10 (2006) 581-588.

[15] S. McIntosh, J.F. Vente, W.G. Haije, D.H.A. Blank, H.J.M. Bouwmeester, Oxygen Stoichiometry and Chemical Expansion of $Ba_{0.5}Sr_{0.5}Co_{0.8}Fe_{0.2}O_{3-\delta}$ Measured by in Situ Neutron Diffraction, Chem. Materials 18, 2006, 2187-2193.

[16] M. Arnold, H. Wang, A. Feldhoff, Influence of CO_2 on the oxygen permeation performance and the microstructure of Perovskite-type $Ba_{0.5}Sr_{0.5}Co_{0.8}Fe_{0.2}O_{3-\delta}$ membranes, J. Membrane Sci., 293 (2007) 44-52.

[17] J. Ovenstone, J. Jung, J.S. White, D.D. Edwards, S.T. Misture, Phase stability of BSCF in low oxygen partial pressures, J. Solid State Chem. 181 (2008) 576–586.

[18] S. Baumann, F. Schulze-Küppers, S. Roitsch, M. Betz, M. Zwick, E.M. Pfaff, W.A. Meulenberg, J. Mayer, D. Stöver. Influence of microstructure on oxygen permeation of $Ba_{0.5}Sr_{0.5}Co_{0.8}Fe_{0.2}O_{3-\delta}$ (BSCF) oxygen transport membranes. J. Membrane Sci. 359 (2010) 102–109.

[19] W. Jin, S. Li, P. Huang, N. Xu, J. Shi. Preparation of an asymmetric perovskite-type membrane and its oxygen permeability. J. Membrane Sci. 185 (2001) 237-243.

[20] X. Chang, C. Zhang, W. Jin, N. Xu. Match of thermal performances between the membrane and the support for supported dense mixed-conducting membranes. J. Membrane Sci. 285 (2006) 232-238.

[21] A. V. Kovalevsky, V. V. Kharton, F. Maxim, A. L. Shaula, J. R. Frade. Processing and characterization of $La_{0.5}Sr_{0.5}FeO_3$-supported $Sr_{1-x}Fe(Al)O_3$-$SrAl_2O_4$ composite membranes. J. Membrane Sci. 278 (2006) 162-172.

[22] O. Büchler, J. M. Serra, W. A. Meulenberg, D. Sebold, H. P. Buchkremer. Preparation and properties of thin $La_{1-x}Sr_xCo_{1-y}Fe_yO_{3-\delta}$ perovskitic membranes supported on tailored ceramic substrates. Solid State Ionics 178 (2007) 91-99.

[23] X. Chang, C. Zhang, X. Dong, C. Yang, W. Jin, N. Xu N. Experimental and modeling study of oxygen permeation modes for asymmetric mixed-conducting membranes. J. Membrane Sci. 322 (2008) 429-435.

[24] K. Watanabe, M. Yuasa, T. Kida, K. Shimanoe, Y. Teraoka, N. Yamazoe. Preparation of oxygen evolution layer/$La_{0.6}Ca_{0.4}CoO_3$ dense membrane/porous support asymmetric structure for high-performance oxygen permeation. Solid State Ionics 179 (2008) 1377–1381.

[25] A. Julian, E. Juste, P. M. Geffroy, V. Coudert, S. Degot, P. Del Gallo, N. Richet, T. Chartier. Elaboration of $La_{0.8}Sr_{0.2}Fe_{0.7}Ga_{0.3}O_{3-\delta}$/$La_{0.8}M_{0.2}FeO_{3-\delta}$ (M= Ca, Sr and Ba) asymmetric membranes by tape-casting and co-firing. J. Membrane Sci. 333 (2009) 132–140.

[26] M. Betz, S. Baumann, F. Schulze-Küppers, W.A. Meulenberg, D. Stöver, Supported oxygen trans-port membranes for oxyfuel power plants. Advances in Science and Technology Vol 72 (2010) 93-98.

[27] E. Gregorová, W. Papst, I. Bohancenko, Characterization of different starch types for their application in ceramic processing. Journal of the European Ceramic Society, 26, 2006, 1301-1309.

[28] W. Schafbauer, R. Kauert, N. H. Menzler and H. P. Buchkremer, Tape casting of anode substrate for SOFCs. CD-ROM Proc. of the 8th Europ. SOFC Forum, Poster B0512, 30.06-04.07.2008, Lucerne, Switzerland.

[29] S. Svarcova, K. Wiik, J. Tolchard, H.J.M. Bouwmeester, T. Grande, Structural instability of cubic perovskite $Ba_xSr_{1-x}Co_{1-y}Fe_yO_{3-\delta}$. Solid State Ionics, 35 (2008) 1787-1791.

[30] A. Leo, S. Liu, J.C. Diniz da Costa, Z. Shao. Oxygen permeation through perovskite membranes and the improvement of oxygen flux by surface modification. Science and Technology of Advanced Materials 7 (2006) 819-825.

[31] S. Haag, A.C. van Veen, C. Mirodatos. Influence of oxygen supply rates on performances of catalytic membrane reactors. Application to the oxidative coupling of methane. C. Today 127 (2007) 157-164.

[32] A. Kovalevsky, C. Buysse, F. Snijkers, A. Buekenhoudt, J. Luyten, J. Kretzschmar, S. Lenaerts. Oxygen exchange-limited transport and surface activation of $Ba_{0.5}Sr_{0.5}Co_{0.8}Fe_{0.2}O_{3-\delta}$ capillary membranes. J. Membrane Sci. 368 (2011) 223-232.

[33] V.V. Kharton, A.V. Kovalevsky, A.A. Yaremchenko, F.M. Figueiredo, E.N. Naumovich, A.L. Shaulo, F.M.B. Marques. Surface modification of $La_{0.3}Sr_{0.7}CoO_{3-\delta}$ ceramic membranes. J. Membrane Sci. 195 (2002) 277-287.

[34] W.K. Hong, G.M. Choi. Oxygen permeation of BSCF membrane with varying thickness and surface coating. J. Membrane Sci. 346 (2010) 353-360.

[35] Z. Shen, P. Lu, G. Yan, X. Hu, Enhancing the oxygen permeability of $Ba_{0.5}Sr_{0.5}Co_{0.8}Fe_{0.2}O_{5+\delta}$ membranes by coating $RBaCo_2O_{5-\delta}$ (R= Pr, Nd, Sm, Gd) layers. Materials Letters 64 (2010) 980-982.

TABLES

Table 1 Overview of literature data for asymmetric membranes.

Membrane material	Layer thickness	$j^{asymmetric}$	$j^{asymmetric} / j^{bulk}$	$L^{bulk} / L^{asymmetric}$	T	Source
	µm	ml $min^{-1}cm^{-2}$	-	-	°C	
$La_{0.6}Sr_{0.4}Co_{0.2}Fe_{0.8}O_3$	200	0.2	3.3	10.0	800	**18**
$SrCo_{0.4}Fe_{0.5}Zr_{0.1}O_3$-0.4MgO	200	0.3	10.0	6.0	900	**19**
$Sr_{1-x}Fe(Al)O_3$-$SrAl_2O_4$	500	0.4	4.0	2.0	900	**20**
$La_{0.58}Sr_{0.4}Co_{0.2}Fe_{0.8}O_3$	20	0.1	1.9	50.0	900	**21, 11**
$SrCo_{0.4}Fe_{0.5}Zr_{0.1}O_3$	200	1.0	1.9	7.5	900	**22**
$La_{0.6}Ca_{0.4}CoO_3$	10	1.5	4.4	100	900	**23**
$La_{0.8}Sr_{0.2}Fe_{0.7}Ga_{0.3}O_3$	80	0.016	5.0	12.5	900	**24**
$Ba_{0.5}Sr_{0.5}Co_{0.8}Fe_{0.2}O_3$	120	1.94	1.3	8.3	900	**25**

Table 2. Estimation of the apparent activation energy ($E_{a,a}$) (kJ mol^{-1}). Q_{Air} = 300 ml(STP) min^{-1}.

	Bare		**O_2 activation layer**	
Q_{Ar} [ml(STP) min^{-1}]	Low T	High T	Low T	High T
200	51.7	32.0	50.9	27.6
300	69.2	35.9	47.6	27.6
400	86.4	36.4	48.1	28.8

FIGURE CAPTIONS

Fig. 1. Slurry preparation for tape casting.

Fig. 2. Fracture cross-sections (SEM pictures) of two membranes after oxygen permeation measurements: (a-b) bare and (c-d) with an oxygen activation layer.

Fig. 3. Details of the morphology of the oxygen activation layer after the permeation test. Fracture cross-section (SEM picture) of the membrane at higher magnification.

Fig. 4. Concentration profiles across the asymmetric membrane thickness and the corresponding model resistances.

Fig. 5. Temperature dependence of the oxygen permeation flux through the bare, supported BSCF thin-film membrane. Synthetic air (21 % v/v O_2) or pure oxygen in the feed stream. Q_{Feed}= 300 ml(STP) min^{-1}, Q_{Sweep} = 300 ml(STP) min^{-1}.

Fig. 6. Temperature dependence of the oxygen permeation flux through the supported BSCF thin-film membranes. Synthetic air (21 % v/v O_2) in the feed stream. Q_{Feed}= 300 ml(STP) min^{-1}. The reduction of polarization effects as a result of the Q_{Sweep} increase makes it possible for surface exchange to become limiting and, therefore, the use of an activation layer has a much stronger impact on the final oxygen flux.

Fig. 7. Effect of the air flow rate. BSCF thin-film membrane with an O_2 activation layer. Different sweep gas flow rate. T = 900 ºC; synthetic air (21 % v/v O_2) in the feed stream.

Fig. 8. Temperature dependence of the oxygen permeation flux through the BSCF thin-film membrane with an O_2 activation layer. Different sweep gas flow rate. Q_{Feed} = 300 ml(STP) min^{-1}.

Fig. 9. Effect of the porous support. BSCF supported thin-film membrane with an O_2 activation layer. T=900 ºC; Q_{Feed} = 300 ml(STP) min^{-1}.

Fig. 10. Temperature dependence of the oxygen permeation using oxygen as a feed and 400 ml(STP) min^{-1} Ar as a sweep gas.

Figure 1

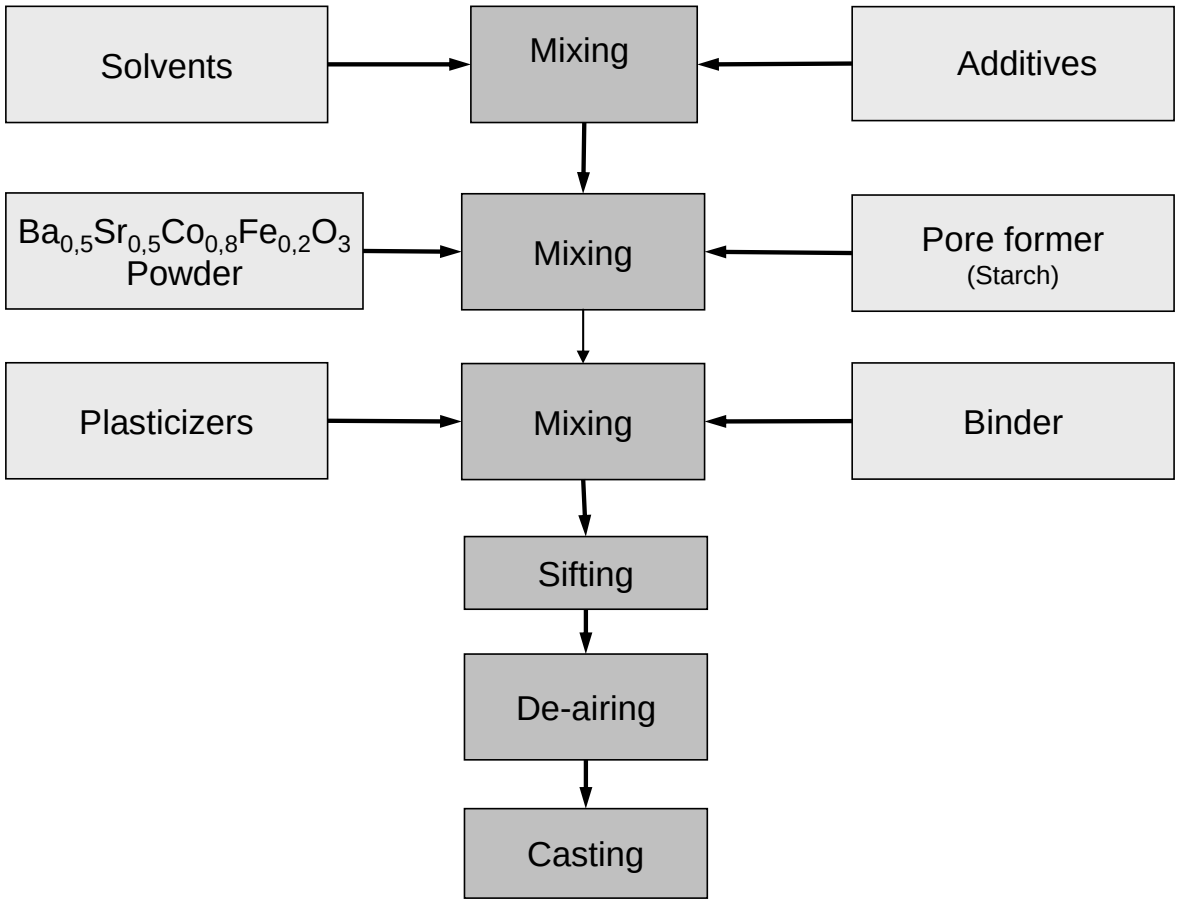
Solvents
Mixing
Additives
$Ba_{0,5}Sr_{0,5}Co_{0,8}Fe_{0,2}O_3$ Powder
Mixing
Pore former (Starch)
Plasticizers
Mixing
Binder
Sifting
De-airing
Casting

Figure 2

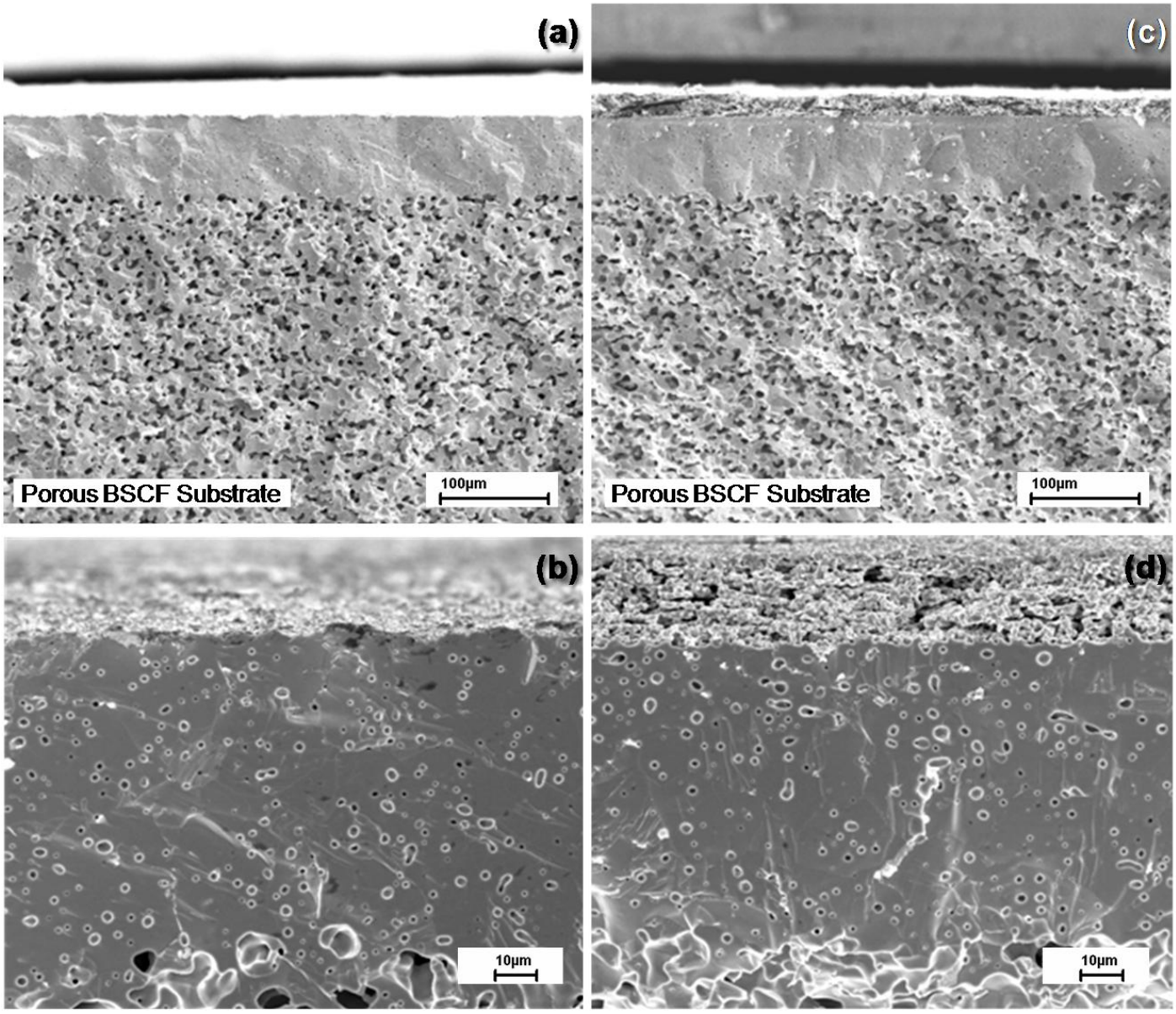
(a)
Porous BSCF Substrate
100μm
(c)
Porous BSCF Substrate
100μm
(b)
10μm
(d)
10μm

Figure 3

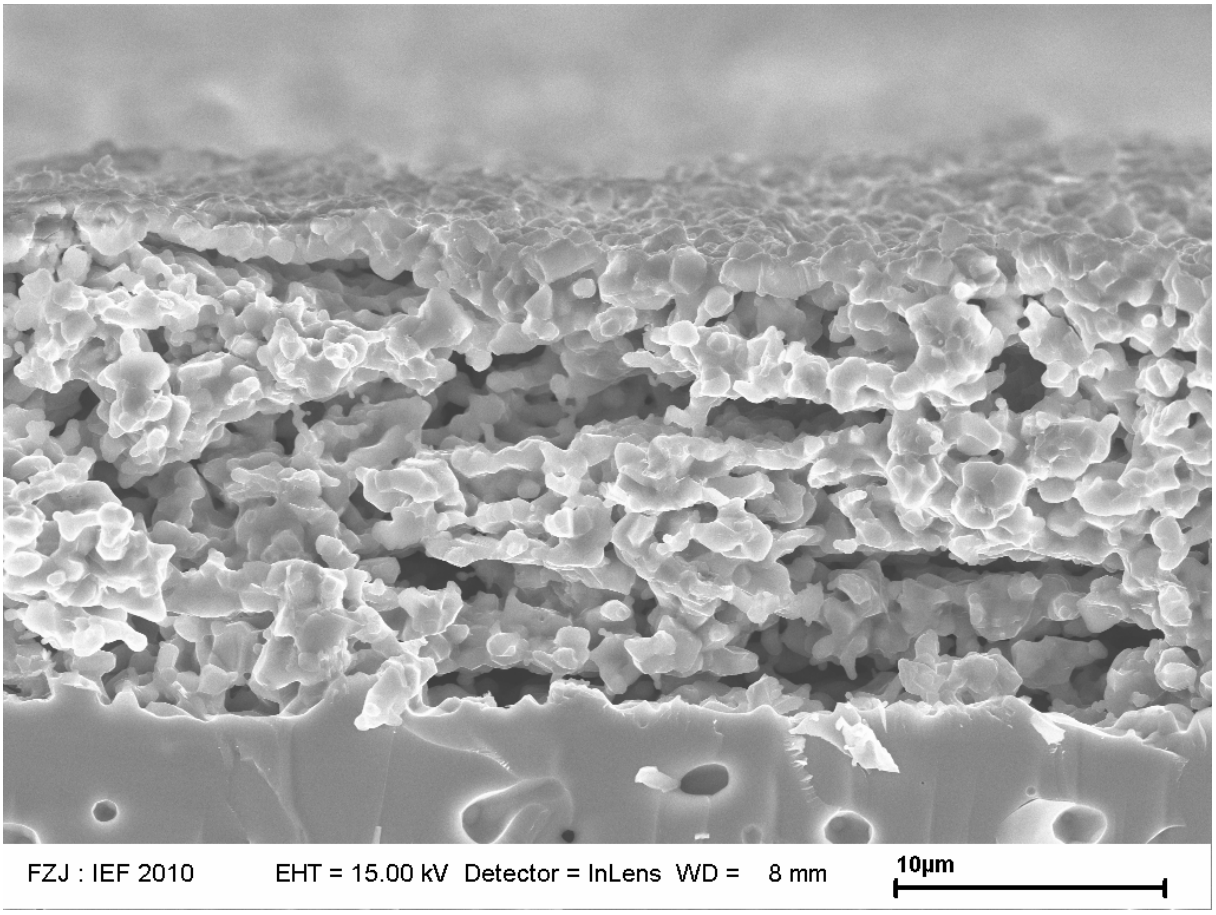

Figure 4

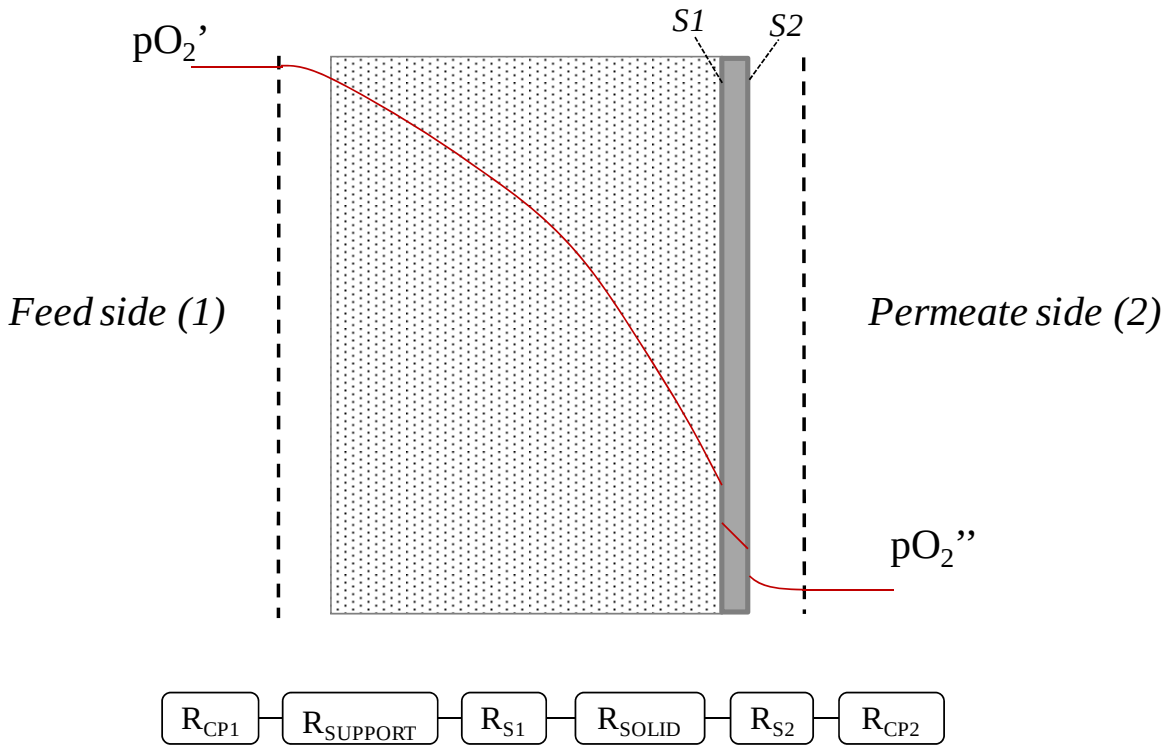
pO2'
S1
S2
Feed side (1)
Permeate side (2)
pO2''
RCP1
RSUPPORT
RS1
RSOLID
RS2
RCP2

Figure 5

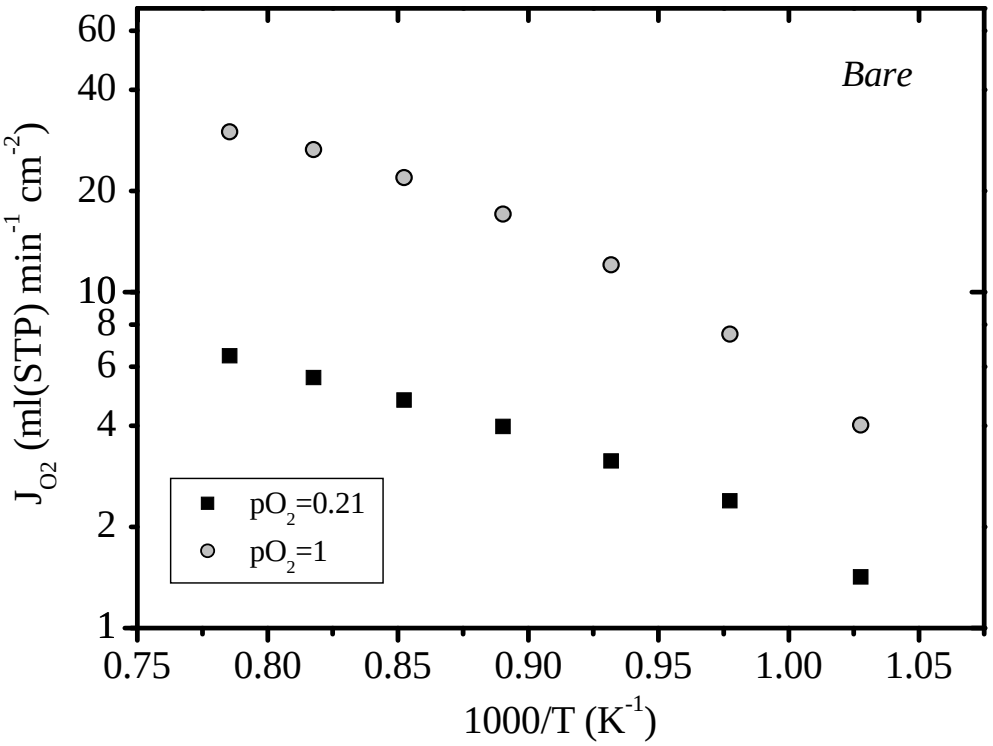
Bare
J_{O2} (ml(STP) min^{-1} cm^{-2})
1000/T (K^{-1})
pO_2=0.21
pO_2=1
60
40
20
10
8
6
4
2
1
0.75
0.80
0.85
0.90
0.95
1.00
1.05

Figure 6

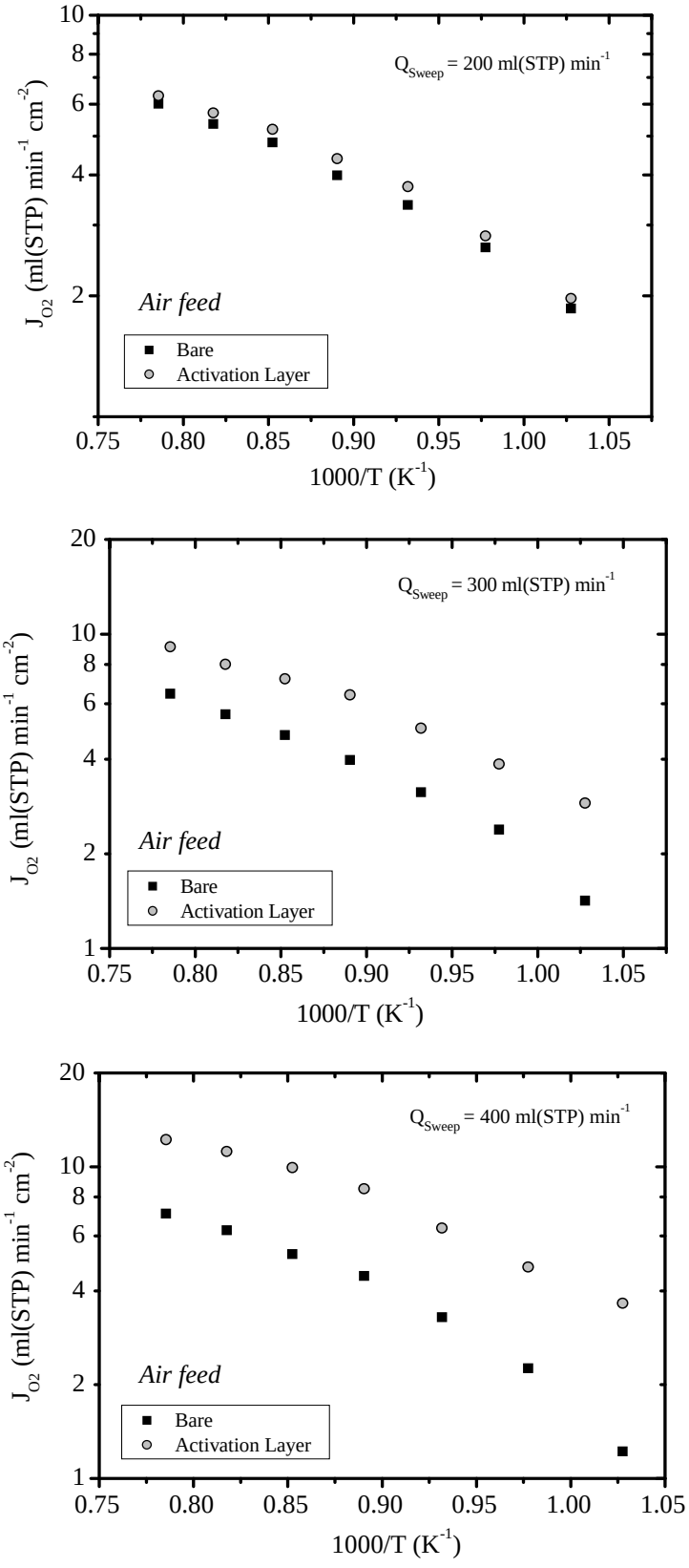
Q_{Sweep} = 200 ml(STP) min^{-1}
J_{O2} (ml(STP) min^{-1} cm^{-2})
1000/T (K^{-1})
Air feed
Bare
Activation Layer
Q_{Sweep} = 300 ml(STP) min^{-1}
J_{O2} (ml(STP) min^{-1} cm^{-2})
1000/T (K^{-1})
Air feed
Bare
Activation Layer
Q_{Sweep} = 400 ml(STP) min^{-1}
J_{O2} (ml(STP) min^{-1} cm^{-2})
1000/T (K^{-1})
Air feed
Bare
Activation Layer

Figure 7

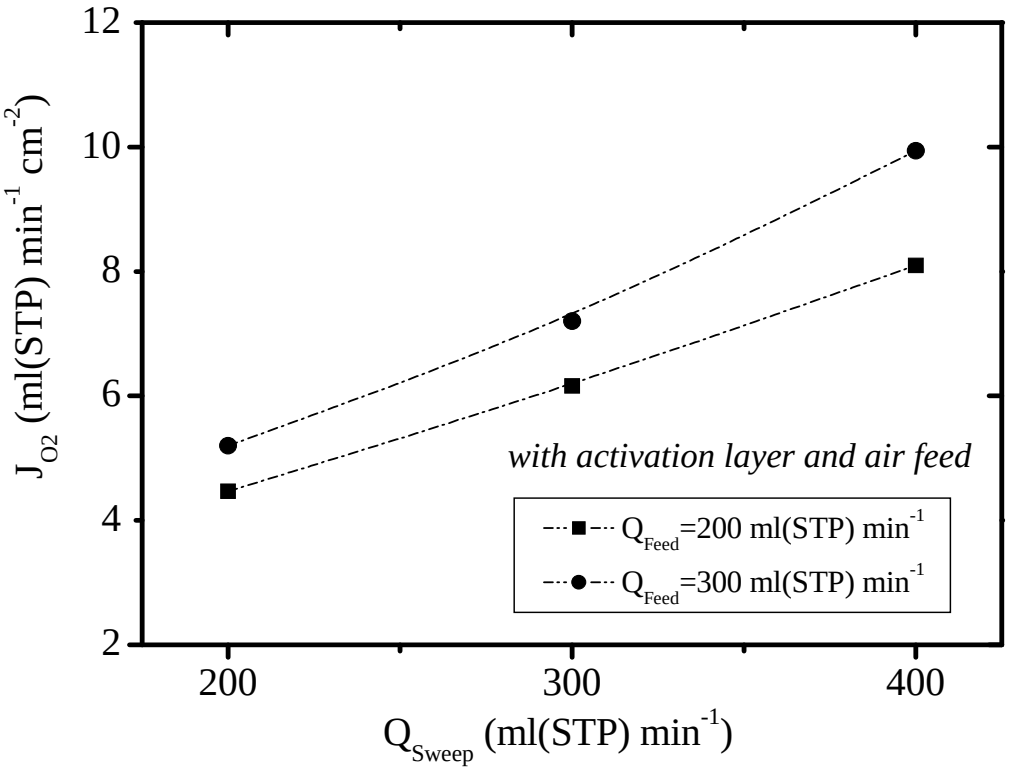
12
10
8
6
4
2
200
300
400
J_{O2} (ml(STP) min^{-1} cm^{-2})
Q_{Sweep} (ml(STP) min^{-1})
with activation layer and air feed
Q_{Feed}=200 ml(STP) min^{-1}
Q_{Feed}=300 ml(STP) min^{-1}

Figure 8

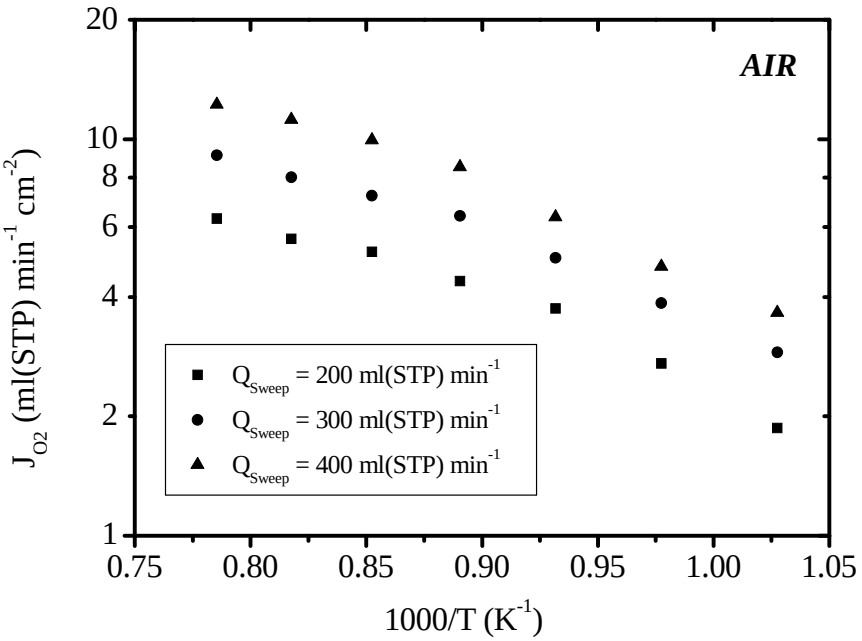
AIR
20
10
8
6
4
2
1
0.75
0.80
0.85
0.90
0.95
1.00
1.05
1000/T (K-1)
J O2 (ml(STP) min-1 cm-2)
QSweep = 200 ml(STP) min-1
QSweep = 300 ml(STP) min-1
QSweep = 400 ml(STP) min-1

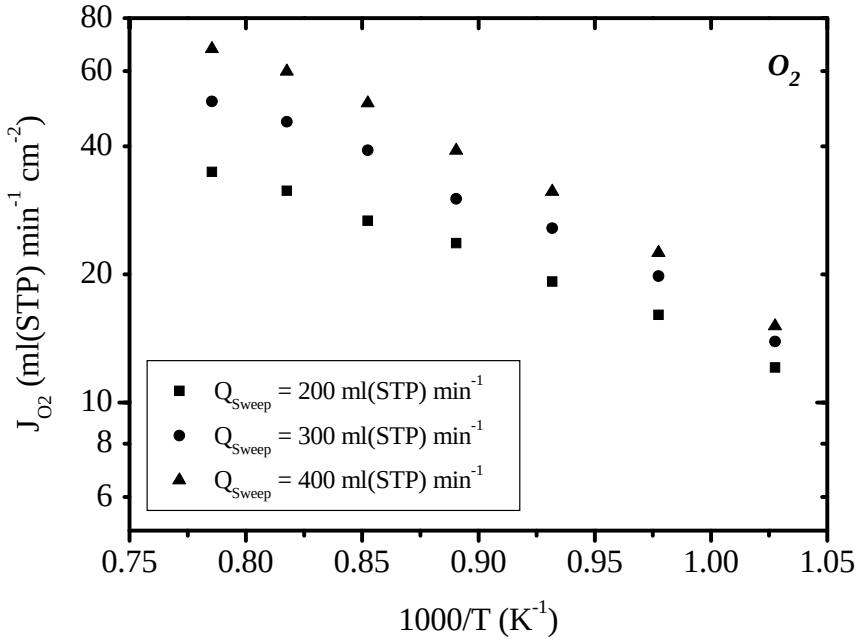
O2
80
60
40
20
10
8
6
0.75
0.80
0.85
0.90
0.95
1.00
1.05
1000/T (K-1)
J O2 (ml(STP) min-1 cm-2)
QSweep = 200 ml(STP) min-1
QSweep = 300 ml(STP) min-1
QSweep = 400 ml(STP) min-1

Figure 9

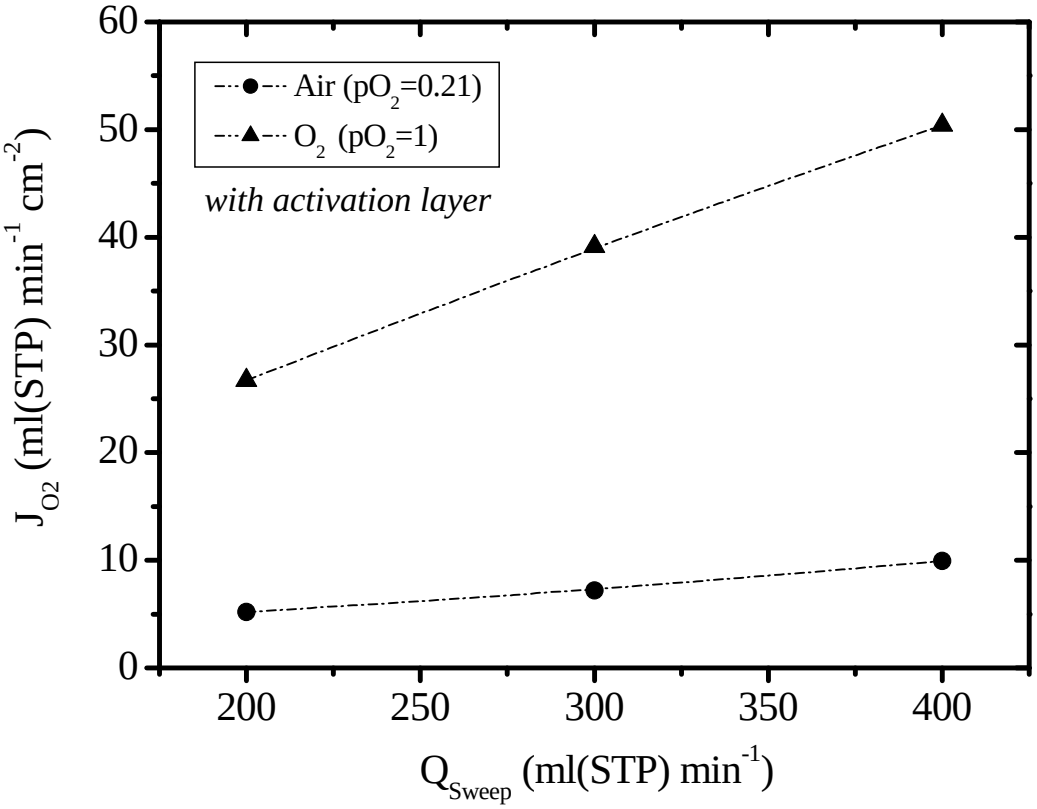
Air (pO2=0.21)
O2 (pO2=1)
with activation layer
JO2 (ml(STP) min-1 cm-2)
QSweep (ml(STP) min-1)
0
10
20
30
40
50
60
200
250
300
350
400

Figure 10

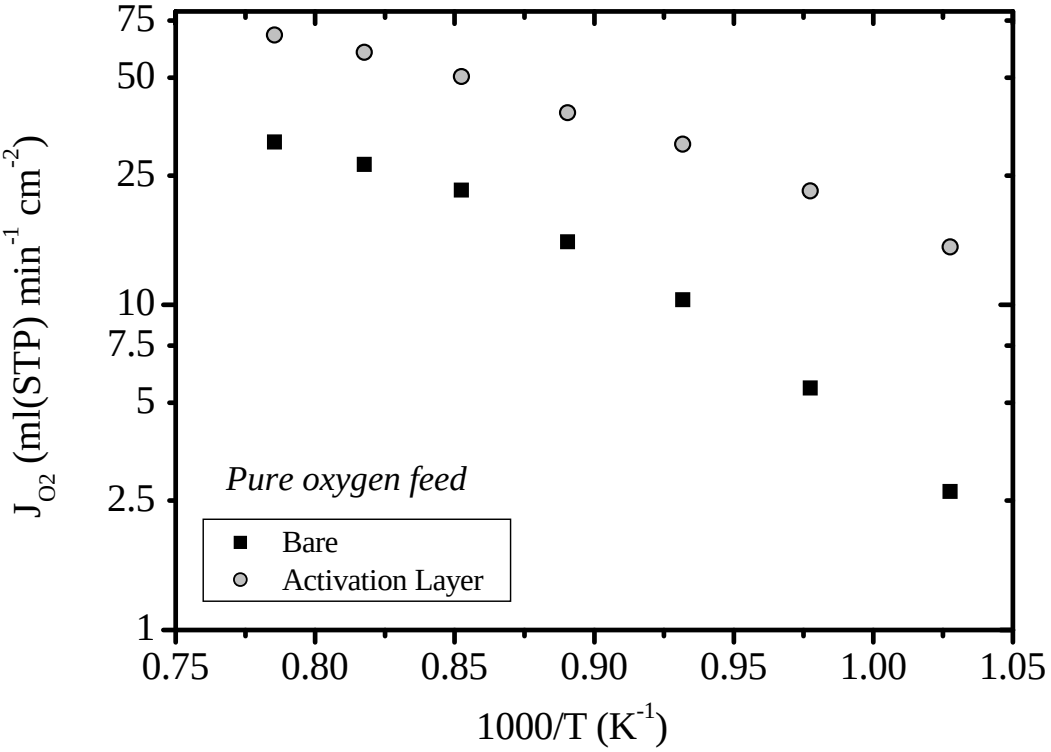
75
50
25
10
7.5
5
2.5
1
0.75
0.80
0.85
0.90
0.95
1.00
1.05
J_{O2} (ml(STP) min^{-1} cm^{-2})
1000/T (K^{-1})
Pure oxygen feed
Bare
Activation Layer